Biosensors and Bioelectronics 26 (2011) 2911–2916

Contents lists available at ScienceDirect

Biosensors and Bioelectronics

journal homepage: www.elsevier.com/locate/bios

Simultaneous topographic and amperometric membrane mapping using an AFM probe integrated biosensor

Sarmiza Elena Stanca[a,c,*], Andrea Csaki[a], Matthias Urban[a], Sandor Nietzsche[b], Christoph Biskup[c], Wolfgang Fritzsche[a,**]

[a] Institute of Photonic Technology, Albert-Einstein-Straße 9, 07745 Jena, Germany
[b] Centre for Electron Microscopy, University Hospital Jena, Ziegelmühlenweg 1, 07743 Jena, Germany
[c] Biomolecular Photonics Group, University Hospital Jena, Teichgraben 8, 07743 Jena, Germany

ARTICLE INFO

Article history:
Received 24 August 2010
Received in revised form 26 October 2010
Accepted 23 November 2010
Available online 1 December 2010

Keywords:
Biosensors
Microcantilever
Peroxidases
Bioelectrocatalysis
Amperometry

ABSTRACT

The investigation of the plasma membrane with intercorrelated multiparameter techniques is a prerequisite for understanding its function. Presented here, is a simultaneous electrochemical and topographic study of the cell membrane using a miniaturized amperometric enzymatic biosensor. The fabrication of this biosensor is also reported. The biosensor combines a scanning force microscopy (AFM) gold-coated cantilever and an enzymatic transducer layer of peroxidases (PODs). When these enzymes are brought in contact with the substrate, the specific redox reaction produces an electric current. The intensity of this current is detected simultaneously with the surface imaging. For sensor characterization, hydroquinone-2-carboxylic acid (HQ) is selected as an intrinsic source of H_2O_2. HQ has been electrochemically regenerated by the reduction of antraquinone-2-carboxylic acid (AQ). The biosensor reaches the steady state value of the current intensity in 1 ± 0.2 s.

1. Introduction

Atomic force microscopy (AFM) can reveal structural details of living cells at a high resolution. To add physiologic value to the morphologic information sensitive scanning techniques capable of recording functional parameters simultaneously with a high resolution in time and space are required. Accordingly, new types of scanning probe microscopy have been created via minuscule electrical devices (Yoo et al., 1997; Champagne et al., 2003; Kocum et al., 2006; Uchihashi et al., 2008). These devices act as high-resolution sensors either by measuring the tensile change in surface stress (Moulin et al., 2000), the adhesion forces (Gu et al., 2005) or by measuring the vertical deflection of the AFM cantilever (Cherian et al., 2003; Karnati et al., 2007; Oliviero et al., 2008; Yue et al., 2008). The integration of a nanoelectrode into an AFM probe, as it is presented in this paper, combines real-time imaging and electrochemical measurements at the nanoscale level. Reported here is the construction and functional characterization of such a miniaturized amperometric biosensor integrated into an AFM cantilever (Fig. 1a and Supporting information Fig. 1).

The sensor consist of an AFM gold-coated probe and an enzymatic layer (PODs) entrapped into poly(o-phenylendiamine) (PPD), which exhibits a high permeability to the analyte and rejects efficiently interfering substances (ÓBrien et al., 2007). PODs catalyze the oxidation of peroxides (Koolmann and Roehm, 2005); also, they catalyze the oxidation of a variety of organic and inorganic compounds at the expense of H_2O_2. Among them, HQ (Holleman and Wiberg, 1995) has been selected as intrinsic source of H_2O_2 (Fig. 1b). HQ is electrochemically regenerated by the reduction of AQ, immobilized on the Au wafer, and fixed on the AFM scanner. When the cantilever is brought in contact with the substrate, the specific enzymatic reaction generates an electric current. The intensity of this current is measured simultaneously while scanning the surface.

2. Materials and methods

2.1. Sensor preparation

All chemicals were purchased from Sigma–Aldrich (Taufkirchen, Germany, puriss. or p.a.), except where otherwise mentioned.

The enzyme has been immobilized on the electrode by entrapping it into a polymer matrix through monomer electropolymerization. Via this method, a PPD film was formed on metallic

* Corresponding author at: Biomolecular Photonics Group, University Hospital Jena, Teichgraben 8, 07743 Jena, Germany. Tel.: +49 3641 9397809; fax: +49 3641 9396602.
** Corresponding author. Tel.: +49 3641 206304; fax: +49 3641 206344.
E-mail addresses: sarmiza.stanca@mti.uni-jena.de (S.E. Stanca), wolfgang.fritzsche@ipht-jena.de (W. Fritzsche).

0956-5663/$ – see front matter © 2010 Elsevier B.V. All rights reserved.
doi:10.1016/j.bios.2010.11.036

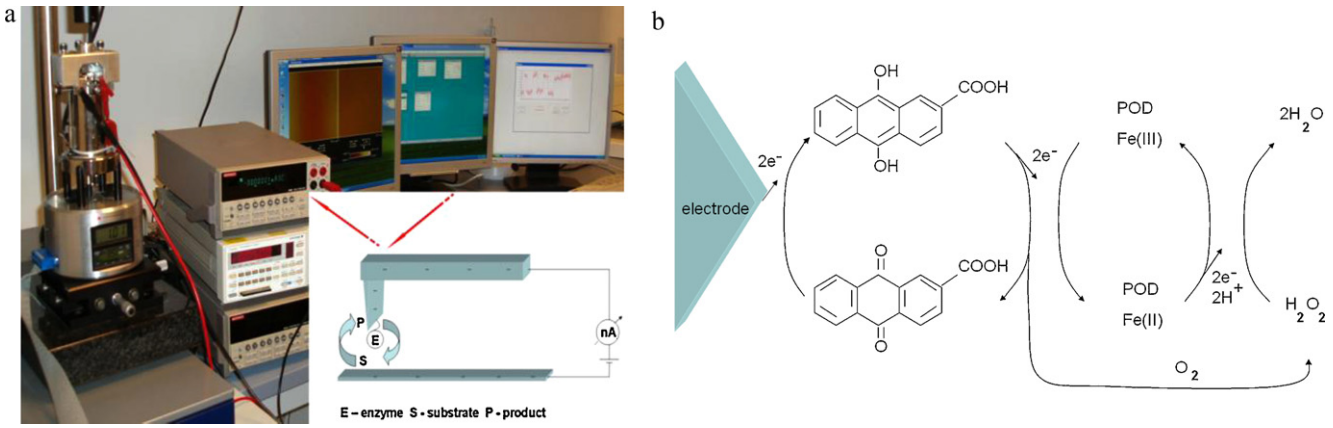

Fig. 1. (a) The experimental set-up. The displays illustrate a simultaneous imaging and amperometrical records. The inset shows the scheme of the AFM probe integrated biosensor. (b) The mediated bioelectrochemical recycling of the POD. The scheme of the experimental set-up.

electrodes, at almost all pH values (Ju et al., 1998). However, POD retains its activity only when it is entrapped at a pH higher than 5 and lower than 7.5. For the film-embedded-enzyme patterned outside of this pH interval, the enzyme does not show activity to hydrogen peroxide. To ensure that POD is not removed from the PPD layer during electrooxidation, we used phosphate buffered saline (PBS, pH 7) to entrap POD close to its isoelectric point of 7.2 (Chance and Maehly, 1955). The voltammograms of 5 mM o-phenylendiamine in buffer solution (PBS) at pH 7 display two broad irreversible oxidation peaks at about +0.35 V and +0.5 to +0.7 V vs. Ag/AgCl, respectively (Supporting information Fig. 2a). At a potential higher than 0.6 V the current does not decrease as expected. This is because the formed polymer PPD is conductive and oxidation of water occurs. In our experiments a potential of 0.65 V vs. Ag/AgCl was chosen to polymerize o-phenylendiamine (Malitesta et al., 1990; Ju et al., 1998; Dixon et al., 2002). The chronoamperometric curves of 5 mM o-phenylendiamine oxidation at 0.65 V vs. Ag/AgCl with and without PODs are accessible in Supporting information. The plots are similar; however, in the first 20 s of the experiment, a little effect of the enzyme on the current is observable. After this time of oxidation, the conductive film is formed at the electrode, and the curves overlap on a plateau of approximate 0.05 μA (Supporting information Fig. 2b). In our experiments we selected an oxidation time of 1 min to form the POD/PPD layer. The immobilization procedure on the gold surface has been completed as follows: a commercial gold contact mode AFM cantilever is positioned into a holder. The cantilever has been previously treated with mesitylene to reduce the water meniscus between the tip and surface (Gu et al., 2005); separately, 100 μL solution of PODs (2 mg PODs in 1 mL of 5 mM o-phenylendiamine phosphate buffer solution (PBS) at pH 7) was dropped on the glass surface, fixed on the AFM scanner. The scanner, insulated with parafilm, has been moved up until the tip was in contact with the drop being held in this position for 1 min and poised at 0.65 V vs. Ag/AgCl for polymerization. Then, the scanner has been moved down and the tip was washed and kept in 0.5 mM H_2O_2 prior to use. Subsequently, the modified cantilever (CAuPODPPD) has been utilized for imaging by operating in a traditional contact mode set-up (Fig. 1a and Supporting information Fig. 1).

The dimension of the electrode critically influences the electric current intensity. Nano-sized electrodes exhibit usually high noise signal. This makes it difficult to extract the actual information, particularly, when bioelectrochemical processes are involved. Small redox changes generated by biolectochemical processes could be easily overlooked in a noisy background. On the other hand, noise filtering could conceal the information. To avoid this, a parallel approach to study the bioelectrocatalytical currents has been conducted with a macro-scaled AuPODPPD electrode. In this manner, the influence of the hydrogen peroxide upon the PODs electrochemistry could be revealed. In the present work the cyclic voltammograms were recorded exclusively with this macro-scaled electrode. All other electrochemical tests were carried out with the nano-scaled electrode.

2.2. Atomic force microscopy

All atomic force micrographs were obtained using a Multimode^{IM} Nanoscope III (Digital Instrument's, Santa Barbara, CA, USA) or a Topometrix Explorer (Veeco, Santa Clara, CA, USA) instrument equipped with contact mode gold tips (Park Scientific Instruments Model No HWMS-06AU). Images were processed using Gwyddion open source software (http://gwyddion.net/). The electrochemical option of the microscope and the custom-made software were accordingly utilized. In our experiments 1 cm^2 gold wafer with a resistivity of 2–4 Ω cm (IPHT Jena) has been used as counter-electrode for operating in AFM. 10 μL of 100 μM AQ, were deposited on the wafer and dried in air. These wafers had previously been heated to 350 °C in air for 4 h, cleaned using a piranha solution (70% H_2SO_4, 30% H_2O_2) and stored under ethanol until required for use. Immediately prior to use they were cleaned again using oxygen plasma (50 W, 5 Pa O_2) for 5 min.

2.3. Electrochemical measurements

Cyclic voltammetry (CV) and chronoamperometry were performed using a computer-assisted potentiostat (Autolab-PGSTAT-100, Eco Chemie, Utrecht, The Netherlands), connected to an electrochemical cell equipped with an Au plate, an Ag/AgCl electrode, against which all potentials were quoted, and an AuPODPPD working electrode.

Steady state amperometric measurements were done as follows: the electrodes were immersed in 5 mL of testing solution at room temperature and poised at the desired value of the applied potential. The calibration curve was constructed by means of measuring the steady-state current for standard aqueous solution of substrate.

2.4. Cell culture

Chinese hamster ovary cells were cultured in alpha-Modified Eagle's Medium (Pan Biotech, Germany) supplemented with 10% fetal bovine serum, 2 mM L-glutamine and 1%

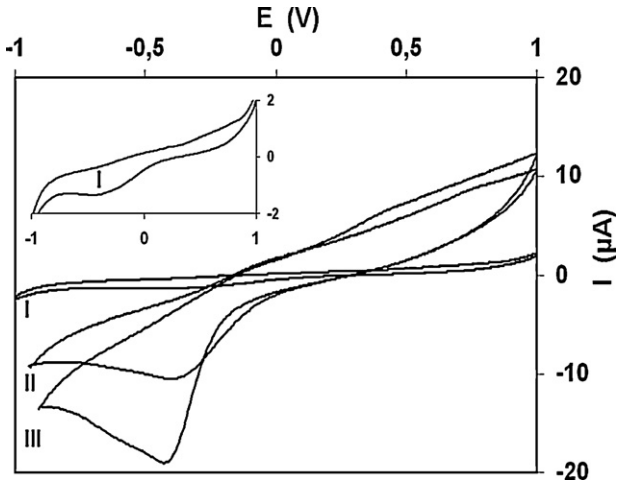

Fig. 2. The bioelectrocatalytic current. The CV of the AuPODPPD electrode at 50 mV/s in PBS pH 7.4 (**I**), in the presence of 0.5 mM AQ (**II**), and in the presence of 0.5 mM H_2O_2 (**III**).

penicillin–streptomycin (Invitrogen). Cells were grown on the coverslips pretreated with L-lysine and kept in a 5% CO_2 environment at 37 °C.

3. Results and discussions

3.1. AuPODPPD biosensor

The investigation of the bioelectrocatalytic currents has been performed with a macro-scaled AuPODPPD electrode. In principle, the cyclovoltammograms could have been directly obtained from measurements with the coated cantilever; however these records would have been too noisy for a thorough evaluation. Since both electrodes were prepared in the same way, we can assume that their distinct difference is the electrode dimension and the bioelectrochemical insights can be more accurate achieved. A significantly higher electrode surface evolving a higher electric current intensity will allow a better assessment of the PODs peroxides system.

3.1.1. The bio-electrocatalytical current

The enzymatic activity of the biosensor, essentially expressed by the bioelectrocatalytic current, has been examined. The CV of the AuPODPPD electrode at a scan rate of 50 mV/s vs. Ag/AgCl illustrates (Fig. 2(I)) the presence of the oxidation and the reduction peaks, which can be attributed to transitions of the iron ions at the catalytic centers of the PODs (Elkaoutit et al., 2008). Similar amplitude of both peaks indicates that the electrochemical processes are reversible, with the connotation of PODs active site regeneration. However, the PODs formal potential value is strongly dependent on the electrode composition (Liu et al., 2006; Elkaoutit et al., 2008; Wang et al., 2010). For this reason, we refrained from a detailed comparison with the literature data.

The influence of AQ and H_2O_2, respectively, upon the PODs CV has been further investigated. Fig. 2 shows the voltammograms of the biosensor cycles from −1 to 1 V vs. Ag/AgCl in phosphate buffer pH 7.4 (**I**), in the presence of 0.5 mM AQ (**II**), or in the presence of 0.5 mM H_2O_2 (**III**). Hydrogen peroxide and AQ, considerably increased the amperometric response, compared with the background current of PODs. The reduction current further increases if the concentration rises from 0.5 mM AQ to 1 mM AQ (data not shown). The current began to rise close to 0 V in every case. These observations indicate that POD catalyzes also the reduction of hydrogen peroxide generated by the oxidation of HQ. The bioelectrode achieved a 95% of the steady-state current in approximate 20 s. This rapid feedback could be explained by a high catalytic activity of the PODs and by the almost unhindered diffusion of H_2O_2 through the PPD layer to the active site of the enzyme. The amperometric biosensor response states a sensor sensitivity of 1.5 ± 0.2 μA/mM. The linear range spans a substrate concentration from 0.05 mM to 1 mM with a correlation coefficient of 0.8639 ($R = 6$). For the apparent Michaelis–Menten constant (K_m^{app}) a value of 0.037 ± 0.003 mM was calculated (Ju et al., 1998). The effect of possible interfering substances on the biosensor current was further estimated. The biosensor response to L-arginine (0.5 mM), L-cysteine (0.5 mM) and ascorbic acid (0.5 mM) attained 80%, 86% and 76%, respectively, of its response to H_2O_2 (100%). These chemicals show an interfering effect; probably they are competitors of the carbon in the electron donation process (Elkaoutit et al., 2008; Wang et al., 2010).

In our AFM experiments, the applied potential (−15 mV to −50 mV) has been more positive than the reduction potential for Fe^{3+}/Fe^{2+} transition in order to identify the pure bioelectrocatalytic current. At the selected potential value, the reduction current could be well attributed to the mediated reduction of the enzyme's complex.

3.2. C-AuPODPPD AFM integrated biosensor

The set-up shown in Fig. 1a and Supporting information Fig. 1 has been used to experiment C-AuPODPPD performance. This custom-made system permits to record, simultaneously, the topography and the electrical properties of the surface. The analogue signal produced at this stage has been converted to a digital signal and output to a display device.

3.2.1. Enzyme loading

The immobilized enzymes possess a number of advantageous features which makes them applicable to such system: (1) their reuse ensures that the same catalytic activity is present for a series of analyses. (2) The enzymes are intrinsically stabilized by the immobilization process. (3) The inactivation of the immobilized enzyme over a period of time is predictable. To estimate the quantity of PODs attached to the tip, it was weighted before and after functionalization yielding a mass of 0.07 ± 0.02 mg. The quantification of the protein content and the enzyme activity is hampered when the enzyme is embedded in polymer on a metallic surface. To this aim, the 3-(4-carboxybenzoyl) quinoline-2-carboxyaldehyde (CBQCA) Protein Quantitation Assay (Invitrogen) and Amplex Red Peroxidase Assays (Invitrogen) have been utilized. All experiments related to enzyme confirmation were conducted in 100 μL volumes with/without cantilever dipped into a quartz cuvette, respectively. The fluorescence was excited at 490 nm and recorded at 525 nm for CBQCA. The Amplex Red fluorescence was excited at 530 nm and recorded at 600 nm. The tests yielded 80 ng/μL protein and 3 μU/μL enzyme activity. The enzyme quantity leached from the cantilever into the solution, during one day of dipping has been below the limit of detection of the method. Each value is an average of 3 measurements. Fluorescence emission spectra were acquired with a Cary Eclipse fluorescence spectrofluorometer (Varian, Darmstadt, Germany) with a slit size of 5 nm for the excitation and emission pathway using Helma quartz cuvettes of 50 μL.

3.2.2. Biosensor response

To examine the biosensor response a control experiment with blank tip has been previously conducted. At this stage, the intensity of the current as function of time has been recorded in the presence (Supporting information Fig. 3a), and in the absence (data not shown), of the substrate. A similar study has been, subsequently, approached using an enzymatic gold cantilever. The curves show the sensor signal recorded with the C-AuPODPPD in the absence

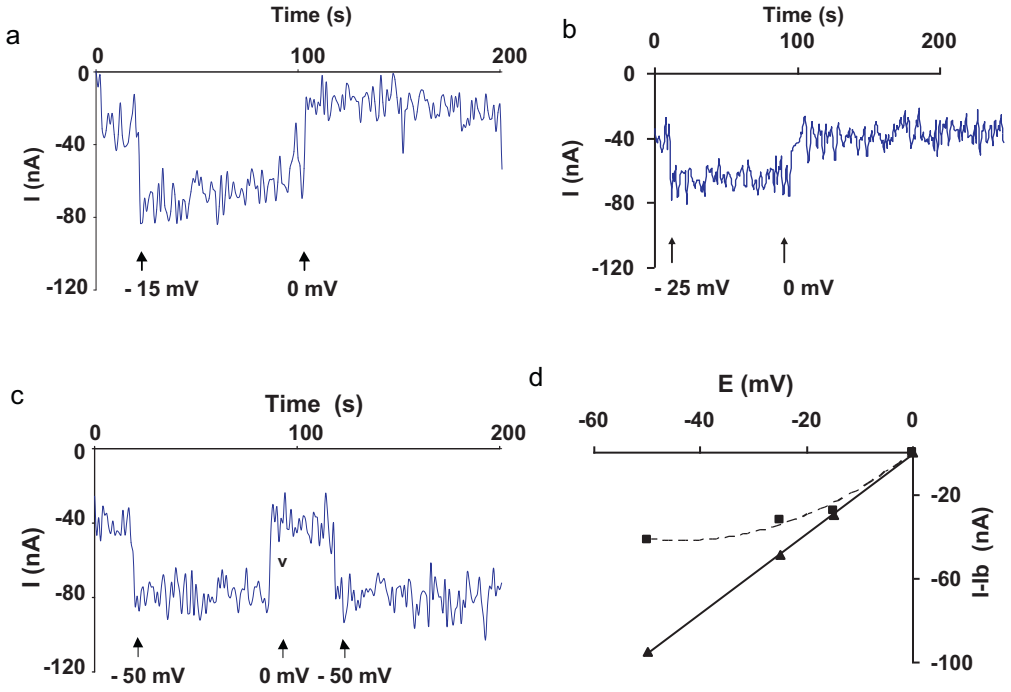

Fig. 3. The influence of the potential on the biosensor response. (a)–(c) The intensity of the current recorded at different potential values as indicated in panels. (d) Hypothetical (straight line) and practical (dashed line) effect of the potential on the current intensity at the same concentration of the substrate. The deviation of the *I–E* plot from the linearity suggests the existence of additional processes.

(b) and in the presence (c) of substrate (Supporting information Fig. 3b–c). Despite of a noisy background, a current intensity of approximate 40 ± 5 nA is observable in panel (c) as a result of enzymatic reaction.

3.2.3. Biosensor response time

The biosensor reaches the steady state value of the current intensity in 1 ± 0.2 s as estimated from amperograms. This relatively small value indicates the presence of the substrate in the vicinity of the enzyme intimately attached to the electrode; consequently, the diffusion does not limit the process. For correlative measurements, the scanning rate of the AFM tip has to be adapted to this value.

3.2.4. Stability and reversibility of the biosensor

The reversibility of the biosensor response has been observed under 4 repetitive potential switches from 0 to −50 mV with the same tip, at the same concentration of substrate, under optimum working conditions previously established. Supporting information Fig. 3d shows the repeatability of the biosensor signal.

3.2.5. Biosensor sensitivity

The electrical signal of the sensor at the assumed molecular recognition is low and superimposed upon a relatively high and noisy baseline. The signal processing normally involves subtracting a reference baseline signal, derived from a similar sensor without any biocatalyst material, from the sample signal.

3.2.6. The influence of the applied potential on the biosensor response

To evaluate this effect the current intensity recorded at different voltages has been plotted as function of potential. Fig. 3 shows the C-AuPODPPD signal at different applied potentials. For an accurate calculation of the effective current intensity, the baseline recorded at 0 mV (Ib (A)) has been subtracted from the values of the apparent current intensity (I(A)) recorded at −15, −25 and −50 mV, respectively. The ohmic linear dependence between current intensity and potential suggests that no enzymatic reaction occurs at the electrode. The deviation of this curve from the expected linear dependence at more negative potentials (35 ± 5 nA at 50 mV, n = 3) suggests the existence of additional processes such as bio-catalytic effects or electrochemical reduction.

3.2.7. The influence of the applied potential on the AFM imaging

The AFM micrograph (Fig. 4a) recorded at the scan rate of 0.02 Hz with the C-AuPODPPD shows a gold wafer modified with AQ. At the stage of AFM scanning, the potential has been switched as presented in Fig. 4d; the biosensor signal has been, accordingly, recorded. Time 0 s is the start of the scan ($x = 0$ μm) and time 3000 s corresponds to the end of the scan ($x = 50$ μm, $y = 50$ μm). The tip scans 512 lines of 50 μm each; thus the total path length covered after scanning an image unidirectionally is 2560 μm. There is no discernible effect from the variable applied voltage on the AFM imaging. Fig. 4b shows the existence of the anodic (at +50 mV) and the cathodic (at −50 mV) currents, which suggests that electrochemical reactions occur in both cases. This method permits to identify the current intensity of every point on the AFM image. The currents shown in Figs. 3 and 4 are recorded with the nano-sized electrode whilst those in Fig. 2, with macro-scaled electrode. This explains the differences in the signal to noise ratios of the recordings.

3.2.8. Bioelectrochemical study of the membrane of CHO cells

To test the performance of the sensor in biological membranes, recordings were also obtained from living CHO cells. Fig 4c shows the AFM micrograph of CHO cells seeded on cover slips coated with poly-L-lysine and superfused with PBS (pH 7.4). Fig. 4f shows the biosensor signal which was obtained at a potential of −50 mV while scanning the image shown in Fig. 4c. Thus, each current recorded at a certain point of time can also be attributed to a pixel in the scan.

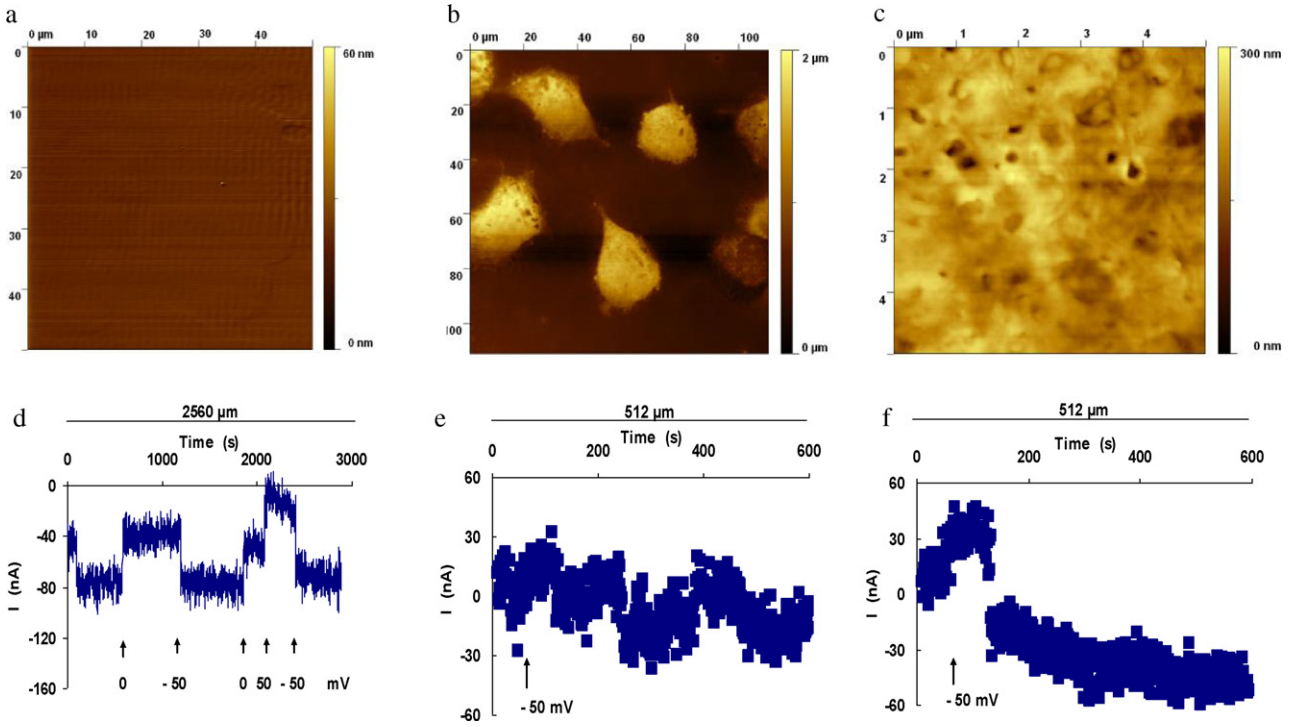

Fig. 4. Application of the biosensor. (a) AFM micrograph of a gold wafer modified with the substrate (b) AFM micrographs of living CHO cells. (c) AFM micrograph of a membrane patch. (d) Recorded biosensor signal obtained while scanning image (a). Time 0 s is the start of the scan ($x = 0$ μm), time 3000 s is the end of the scan ($x = 2560$ μm). (e, f) Recorded biosensor signal obtained while scanning image (c) at a potential of −50 mV vs. Ag/AgCl in the absence (e) and the presence (f) of POD. Time 0 s corresponds to $x = 0$ μm and time 600 s corresponds to 512 μm of the scan.

The existence of the reductive current at −50 mV in the absence of H_2O_2 can only be explained by the bio-electrochemical reduction of the PODs by interaction with the membrane. The blank sensor running in the same condition spans a current intensity from $+20 \pm 5$ nA to -30 ± 5 nA (Fig. 4e). The statistical evaluation relies on 3 measurements. Moreover, the biosensor records a positive current in the absence of the applied electrical potential; this fact can be associated with the oxidative process catalyzed by the PODs. Further control experiments in a flow-cell exploring the reaction dependence on the pH, ionic strength, temperature and inhibitor concentrations are critically required. Exploring the enzyme variety this technique could find wide bio-analytical application despite its limitations set by the narrow voltage range. This multimodal and spatially with nanometer precision resolved study of cell membrane function represents a promising practical application of the introduced methodical development.

4. Conclusions

Reported here is the construction of a miniaturized peroxide amperometrical biosensor integrated into an AFM cantilever. The sensor consists of an AFM gold-coated cantilever and an enzymatic transducer layer (PODs) entrapped into poly (o-phenylendiamine) (PPD). Hydroquinone-2-carboxilic acid has been utilized as intrinsic source of H_2O_2. The AFM equipped with blank or functionalized tip has been operated in contact mode with a custom-made electrochemical option. The biosensor reaches the steady state value of the current intensity in 1 ± 0.2 s. Subsequently, a preliminary study with this biosensor of the CHO cell membrane was attempted. The existence of the reductive current on the membrane at an applied potential of −50 mV vs. Ag/AgCl demonstrates the bio-electrochemical reduction of the PODs by the cell membrane. Finally, we note that this method allows to attribute the current intensity to each point of the AFM image of living cells.

Acknowledgements

The DAAD fellowship (FKZ A/09/02568) for Dr. Stanca is gratefully acknowledged. We thank Dr. Frank Garwe for valuable discussions. We thank also Karin Schoknecht for the cell culture and Dipl. Ing. Janina Wirt for the AFM set-up photo.

Appendix A. Supplementary data

Supplementary data associated with this article can be found, in the online version, at doi:10.1016/j.bios.2010.11.036.

References

Champagne, A.R., Couture, A.J., Kuemmeth, F., Ralph, D.C., 2003. Appl. Phys. Lett. 82 (7), 1111–1113.
Chance, B., Maehly, A.C., 1955. Methods Enzymol. 2, 764–775.
Cherian, S., Gupta, R.K., Mullin, B.C., Thundat, T., 2003. Biosens. Bioelectron. 19, 411–416.
Dixon, B.M., Lowry, J.P., OïNeill, R.D., 2002. J. Neurosci. Methods 119, 135–145.
Elkaoutit, M., Naranjo-Rodriguez, I., Dominguez, M., Hernandez-Artiga, M.P., Bellido-Milla, D., Hildago-Hildago de Cisneros, J.L., 2008. Electrochim. Acta 53, 7131–7137.
Gu, J., Xiao, Z., Yam, C.-M., Qin, G., Deluge, M., Boutet, S., Cai, C., 2005. Biophys. J. Biophys. Lett. 89 (5), L31–L33.
Holleman, A.F., Wiberg, N., 1995. Lehrbuch der Anorganischen Chemie 101. Auflage, de Gruyter, Berlin, pp. 531–538.
Ju, H., Zhou, D., Yiao, Y., Chen, H., 1998. Electroanalysis 10, 541–545.
Karnati, C., Du, H., Ji, H.-F, Xu, X., Lvov, Y., Mulchandani, A., Mulchandani, P., Chen, W., 2007. Biosens. Bioelectron. 22, 2636–2642.
Kocum, C., Ülgen, S.D., Cubukcu, E., Piskin, E., 2006. Ultramicroscopy 106, 326–333.
Koolmann, J., Roehm, K.H., 2005. Color Atlas of Biochemistry, 2nd ed. Thieme, Stuttgart/New York, pp. 88–110.
Liu, Y., Yuan, R., Chai, Y., Tang, D., Dai, J., Zhong, X., 2006. Sens. Actuators B 115, 109–115.

Malitesta, C., Palmisano, F., Torsi, L., Zambolin, P.G., 1990. Anal. Chem. 62, 2735–2740.
Moulin, A.M., OïShea, S.J., Welland, M.E., 2000. Ultramicroscopy 82, 23–31.
ÓBrien, K.B., Killoran, S.J., ÓNeill, R.D., Lowry, J.P., 2007. Biosens. Bioelectron. 22, 2994–3000.
Oliviero, G., Bergese, P., Canavese, G., Chiari, M., Colombi, P., Cretich, M., Damin, F., Fiorilli, S., Marasso, S.L., Ricciardi, C., Rivolo, P., Depero, L.E., 2008. Anal. Chim. Acta 630, 161–167.
Uchihashi, T., Ramsperger, U., Nakayama, T., Aono, M., 2008. Jpn. J. Appl. Phys. 47, 1797–1799.
Wang, J., Yuan, R., Chai, Y., Li, W., Fu, P., Min, L., 2010. Colloids Surf. B 75, 425–431.
Yoo, M.J., Fulton, T.A., Hess, H.F., Willett, R.L., Dunkleberger, L.N., Chichester, R.J., Pfeiffer, L.N., West, K.W., 1997. Science 276, 579–582.
Yue, M., Stachowiak, J.C., Lin, H., Datar, R., Cote, R., Majumdar, A., 2008. Nano Lett. 8, 520–524.